Noname manuscript No.
(will be inserted by the editor)

Nitriding of 4H-SiC by irradiation of fourth harmonics of Nd:YAG laser pulses in liquid nitrogen

Masaharu Shimabayashi · Takuma Kaneko · Koichi Sasaki*

Received: date / Accepted: date

Abstract This study presents surface nitriding of 4H-SiC by the irradiation of the fourth harmonics of Nd:YAG laser pulses in liquid nitrogen. A nitride layer with a depth of 1 μm is formed on the irradiated area. The irradiated area has a bumpy morphology. On the other hand, we also find a nitride layer with a smooth surface morphology in the outside of the irradiated area. The concentration of nitrogen is dependent on the laser fluence, and is 1%-5%. The diffusion coefficient of nitrogen, which is deduced from the depth profile of the nitrogen number density, is much greater than the diffusion coefficient in solid SiC, suggesting the transport of nitrogen in melted SiC. Considering the fact that SiC does not have a melted state at the atmospheric pressure, it is revealed by the present work that the melted SiC is realized transiently with the help of the high pressure driven by the laser irradiation.

Keywords surface nitriding · 4H-SiC · laser irradiation · liquid nitrogen

1 Introduction

Semiconductor power devices are utilized in various scenes in recent years. A typical example is power transistors used in inverter and convertor modules. The improvement of the energy efficiency and the upper-limit voltage of power semiconductor devices is important to construct the energy-saving society. At the moment, the majority of power semiconductor devices utilizes silicon. However, the performance of Si-based power transistors has been reaching its theoretical limit in recent years. For this reason, the expectation is focused on SiC as a next-generation power semiconductor. Because of a wide band gap of 3.26 eV, SiC-based power semiconductor devices can have advantages in the high voltage insulation strength and the robustness against high temperature [1–3]. In addition, SiC-based

* Corresponding author

K. Sasaki
Division of Applied Quantum Science and Engineering, Hokkaido University
Kita 13, Nishi 8, Kita-ku, Sapporo 060-8628, Japan
E-mail: sasaki@qe.eng.hokudai.ac.jp

metal-oxide-semiconductor field-effect transistors (MOSFETs) have potential advantages in their low on-resistance and high switching speed [4–6]. However, the on-resistance of SiC-based MOSFETs under development is much higher than the theoretical expectation.

A reason for the high on-resistance of SiC-based MOSFETs is the low carrier mobility in the channel region under the gate insulation film [7–9]. The low carrier mobility results from defects around the interface between the channel region and the gate insulation film. Therefore, it is required to develop a method to passivate the surface of SiC before depositing the gate insulation film. A first-principle calculation suggests that the nitriding of the SiC surface can be a solution to this problem [10]. In previous works, we examined the surface nitriding of 4H-SiC by the irradiation of a remote nitrogen plasma [11,12]. A nitride layer with a thickness of 5 nm was formed on the surface of 4H-SiC, but this method had a problem of the decrease in the carbon concentration by the formation of volatile molecules such as C_2N_2. The significant amount of oxygen contamination at the top surface was also a problem.

In many years ago, we reported an experiment on the formation of nitride layer on titanium and the production of TiN nanoparticles by laser ablation of a titanium target in liquid nitrogen [13–15]. A technical advantage of the nitriding process in liquid nitrogen is that it does not need a vacuum chamber. In addition, we may expect high nitriding reactivity because of the denser ambient medium than the nitrogen plasma. In this work, we repeated a similar experiment by using 4H-SiC and the fourth harmonics of Nd:YAG laser pulses.

In this paper, we report the depth profile of the nitrogen concentration on the 4H-SiC sample irradiated with the laser pulses, and discussed the formation mechanism of the nitride layer. This paper is composed as follows. In the following section, Sec. 2, we report the arrangements of the present experiment. The results obtained using the experimental arrangement are described in Sec. 3. Section 4 is devoted to discussion on the experimental results. Conclusions of the present study are summarized in Sec 5.

2 Experimental method

The experimental setup is schematically shown in Fig. 1. The container of liquid nitrogen was made of stainless steel, and the outside of the liquid nitrogen container was surrounded by a vacuum vessel for the thermal isolation. The vacuum vessel was evacuated using a turbo molecular pump below 1×10^{-5} Torr. A 4H-SiC target with a size of 14×14 mm^2 was immersed in liquid nitrogen. The sample was rinsed with 5% hydrogen fluoride solution for 10 min before introducing it into liquid nitrogen to remove the native oxide. We investigated the nitriding characteristics of the carbon-side surface (C-face) of 4H-SiC in this experiment, since it is reported that MOSFETs constructed on the C-face have a higher channel mobility than that constructed on the Si-face [16,17]. The vacuum vessel and the liquid nitrogen container had optical windows to launch the laser beam and to observe the target region. We employed the fourth harmonics of a Nd:YAG laser (Spectra-Physics, INDI) at a wavelength of 266 nm in this experiment. The fourth harmonics was necessary to realize the deposition of the laser energy onto the target, since the target was transparent against the laser beam if its photon energy

did not exceed the band gap of SiC. The laser energy was 40 mJ/pulse. The laser beam was focused using a lens with a focal length of 7 cm, which was installed in the vacuum vessel, onto the sample surface from the normal direction. The position of the SiC target was movable along the optical axis of the laser beam, so that the laser fluence on the target surface was varied between 0.05 and 9.9 J/cm^2 (the spot size of the laser beam was varied between 0.72 and 10 mm). The repetition frequency and the duration of the Nd:YAG laser pulses were 10 Hz and 10 ns, respectively. The duration of the laser irradiation was 3 min (1800 laser pulses in total). After the irradiation, the sample was pulled up to the atmosphere, and was transferred to analyses. The atomic composition on the sample surface was analyzed by X-ray photoelectron spectroscopy (XPS), and the weight density of the sample surface was analyzed by X-ray reflectometry (XRR). The spot size in the XPS measurement was 1 mm. A secondary electron microscope (SEM) was used for examining the surface morphology of the sample.

3 Results

Figure 2 shows SEM images of the surface of the 4H-SiC sample. A crater with an area size of 0.64 mm^2 was formed on the sample surface, as shown in Fig. 2(a). The crater had a clear boundary, suggesting that the scattering of the laser beam by small bubbles in liquid nitrogen was negligible in the present experiment. The laser fluence, which was estimated by dividing the laser energy by the crater area, was 6.2 J/cm^2. As shown in the magnified images (Figs. 2(b) and 2(c)), the surface of the ablation crater had a bumpy morphology. Each grain had a size of several micrometers. The depth of the crater, which was measured using a laser scanning microscope, was approximately 70 μm. This depth corresponded to an etching rate of $\sim$ 40 nm/pulse since it was formed by the irradiation of 1800 laser shots.

The concentration of nitrogen at the top surface of the crater, which was examined by XPS, was dependent on the laser fluence as shown in Fig. 3. The nitrogen concentration increased with the laser fluence, and it was saturated at a laser fluence of $\sim$ 5 J/cm^2. The maximum nitrogen concentration we observed was 5%, which was much lower than the chemical composition in Si_3N_4 and C_3N_4. Figure 4 shows the depth profiles of atomic concentrations, which was obtained by XPS combined with Ar^+ beam sputtering. We detected nitrogen even at a depth of 1 μm from the surface. The depth profile of the nitrogen concentration was almost flat at the center of the ablation crater (0 mm), as shown in Fig. 4(a). The depth region within 200 nm from the surface was contaminated by oxygen, and a low concentration of silicon was observed in this region. The source of oxygen may be dissolved molecular oxygen in liquid nitrogen. This speculation is supported by the experimental result that a lower oxygen concentration was observed when the gas phase above liquid nitrogen was filled with nitrogen during the laser irradiation. On the other hand, the carbon concentration was lower than 50% in the entire depth region except the top surface, where the carbon concentration is usually enhanced by the contamination. The lower concentration of carbon than silicon was also observed in the surface nitriding of 4H-SiC using a remote nitrogen plasma [11,12], and the mechanism was estimated to be desorption of volatile molecules such as C_2N_2. We also observed the nitride layer in the outside of the crater, as shown in Fig. 4(b), which was observed at a lateral distance of 1 mm

from the center of the ablation crater. The maximum lateral distance where we observed the nitride layer was approximately 2 mm from the crater center. It is noted that, as shown in Fig. 2(a), the outside region of the crater had a smooth surface morphology. The smooth surface morphology is useful for the application to the fabrication process of MOSFETs. The oxygen contamination and the low silicon concentration in the depth region of $\leq$ 200 nm were also observed in the outside of the crater. The carbon concentration was also lower than 50% in the entire depth region. On the other hand, in contrast to the depth profile at the crater center, the nitrogen concentration decreased with the depth in the outside region of the crater, as shown in Fig. 4(b).

Figure 5 shows the depth profiles of the weight densities, which were evaluated by XRR at the crater center and at a lateral distance of 1 mm from the crater center. The weight density of virgin 4H-SiC, which is 3.2 g/cm^3, is indicated by the horizontal dashed line in the figure. The ambiguity in the evaluation of the weight density from the XRR profile was estimated to be 0.5 g/cm^3. It is understood from Fig. 5 that the region with a depth of 1.3 μm from the surface was affected by the laser irradiation. This depth region had lower weight densities, especially inside the ablation crater. This result indicates the desorption of silicon and carbon from the sample by the laser irradiation. By combining the depth profiles of the atomic concentrations shown in Fig. 4 and the weight density shown in Fig. 5, we evaluated the depth profile of the number density of atomic nitrogen as shown in Fig. 6. The outside region of the ablation crater contained more amount of atomic nitrogen. The density of atomic nitrogen was almost flat inside the ablation crater, while it decreased with the depth in the outside of the crater.

4 Discussion

The formation of the crater shown in Fig. 2 indicates that the laser fluence of 6.2 J/cm^2 exceeds the threshold for laser ablation of 4H-SiC. The threshold for laser ablation was roughly $\sim$ 1 J/cm^2. The reason for the constant nitrogen concentration in the depth profile in the crater center (Fig. 4(a) and Fig. 6) may be the ablation removal of the depth region with a high nitrogen concentration. The lower nitrogen concentration inside the crater is also attributed to the ablation removal. The significant decrease in the weight density on the crater surface shown in Fig. 5 is consistent with the ablation removal of the top surface. However, the formation of the nitride layer on the crater surface reveals that the etching depth by laser ablation is shallower than the depth with the transport of nitrogen. In other words, a part of the depth region with the transport of nitrogen remains on the sample surface. The morphology of the crater surface shown in Figs. 2(b) and 2(c) suggests high temperature cracking which was caused by the melting and the coagulation in the remained depth region. On the other hand, the smooth surface morphology indicates no ablation removal in the outside of the crater. This means that the temperature in the outside area of the crater is lower than that in the inside with the high temperature cracking. The no ablation removal may result in the decrease in the nitrogen concentration with the depth (Fig. 4(b) and Fig. 6). However, the slight decrease in the weight density shown in Fig. 5 indicates that the desorption of species from the sample is not negligible even in the outside area of the crater.

We try to estimate the diffusion coefficient of nitrogen in 4H-SiC, under the assumption that the dominant transport mechanism of nitrogen is diffusion. We assume that the number density of nitrogen at the top surface is constant and the SiC sample has a semi-infinite depth. The solution of the one-dimensional diffusion equation is given by [18]

$$n(x) = n_0 \mathrm{erfc}\left(\frac{x}{2\sqrt{D_\mathrm{N}\Delta t}}\right), \tag{1}$$

where $n(x)$ is the number density of nitrogen at depth x from the surface, Δt is the duration of diffusion, and D_N is the diffusion coefficient. Since eq. (1) ignores the temperature gradient, the diffusion coefficient deduced on the basis of eq. (1) gives us the estimation on the order of magnitude. Figure 7 shows the normal probability plot of the depth profile of the nitrogen number density observed at a lateral distance of 1 mm from the crater center (the same data as those plotted in Fig. 6). A straight line is found in the normal probability plot, as shown in Fig. 7, and as a result, we have evaluated that the diffusion coefficient for nitrogen in 4H-SiC is $D_\mathrm{N} \simeq 5 \times 10^{-11}$ cm^2/s. In this estimation, we substituted $\Delta t = 180$ s (3 min) for the duration of diffusion. However, the duration of diffusion in the reality is much shorter than 180 s, since the laser irradiation is intermittent (pulsed) at a repetition frequency of 10 Hz with a pulse duration of 10 ns. Therefore, $D_\mathrm{N} \simeq 5\times10^{-11}$ cm^2/s gives us the lower limit for the diffusion coefficient. According to our simplified heat conduction calculation, the duration of the high sample temperature ($\geq$ 2000 K), which is induced by the pulsed laser irradiation, is estimated to be $\sim$ 10 μs. If we assume $\Delta t = 18$ ms (10 μs $\times$1800 laser shots) for the duration of diffusion, the diffusion coefficient is estimated to be $D_\mathrm{N} \simeq 5 \times 10^{-7}$ cm^2/s.

The diffusion coefficient of nitrogen in SiC has been investigated by several authors. Kroko and Milnes reported $10^{-16} - 10^{-13}$ cm^2/s at sample temperatures between 2300 and 2800 K [19], whereas Neudeck reported $2 \times 10^{-13} - 5 \times 10^{-12}$ cm^2/s at sample temperatures between 1800 and 2450 K [20,21]. The diffusion coefficient estimated by the present experiment is higher than these literature values even if we assume $\Delta t = 180$ s for the duration of diffusion. On the other hand, the diffusion coefficients observed in laser doping experiments by Tian *et al.* [21] and Ikeda *et al.* [22] are 3.9×10^{-7} and 5.7×10^{-6} cm^2/s, respectively, which are rather similar to $D_\mathrm{N} \simeq 5 \times 10^{-7}$ cm^2/s in the present work when assuming $\Delta t = 18$ ms.

It is known that SiC does not have a melted state with the same atomic composition of Si/C = 1/1 at the atmospheric pressure [23]. However, liquid SiC is predicted by Togaya and Sugiyama in a highly pressurized condition at a temperature higher than 3000 K [24]. It is well known that a pressure wave is generated in the target when it is ablated by a laser pulse, and as a result, a high-pressure, high-temperature state is realized in the target transiently [25,26]. The transient high pressure is especially emphasized when the target is ablated in a liquid environment. Considering the morphology on the crater surface, it is speculated that the SiC sample is melted transiently with the help of the high pressure driven by laser ablation. If the surrounding region of the crater exceeds the phase transition temperature, the high diffusion coefficient can be explained by diffusion in melted SiC. Another explanation for the high diffusion coefficient is the transport of nitrogen in vaporized target materials (Si and C). However, we believe that this

transport mechanism is unlikely, since the surface formed by the redeposition of vaporized species may have a roughened morphology. The smooth surface morphology with the higher nitrogen concentration may be realized at the optimum temperature where the high diffusion coefficient is compatible with the no ablation removal.

5 Conclusions

A nitride layer on a 4H-SiC surface is useful to avoid defects in the channel region of SiC-based MOSFETs. In this work, we examined surface nitriding of 4H-SiC by the irradiation of the fourth harmonics of Nd:YAG laser pulses in liquid nitrogen. A nitride layer with a depth greater than 1 μm was formed on the ablation crater as well as the surrounding region. The crater surface had a bumpy morphology, while the surface of the nitride layer formed on the surrounding region of the crater was smooth. The bumpy morphology of the crater surface indicates the melting and the coagulation of the sample. The nitrogen concentration at the crater was lower than that in the surrounding region, which may be due to the ablation removal of the top surface in the crater region. The diffusion coefficient evaluated from the depth profile of the nitrogen number density, which was observed in the outside region of the crater, was much higher than the diffusion coefficient of nitrogen in solid SiC. The high diffusion coefficient suggests the transport of nitrogen in melted SiC even in the outside area of the ablation crater. The melted SiC may be realized with the help of the high pressure driven by the laser irradiation. The laser irradiation onto 4H-SiC is not applicable to the fabrication process of SiC-based MOSFETs without any changes. However, the present work gives us the novel insight into the fundamentals of the transient phase change driven by the pulsed heating.

Acknowledgements The authors would like to thank Prof. N. J. Vasa for useful discussion. This work was supported by Grant-in-Aid for JSPS Fellows from Japan Society for the Promotion of Science (JSPS).

Conflict of interest

On behalf of all authors, the corresponding author states that there is no conflict of interest.

References

1. K. Ito, S. Tsukimoto, and M. Murakami, Effects of Al ion implantation to 4H-SiC on the specific contact resistance of TiAl-based contact materials. Sci. Technol. Adv. Mater. **7**, 496 (2006)
2. A. Frazzetto, F. Giannazzo, R. L. Nigro, V. Raineri, and F. Roccaforte, Structural and transport properties in alloyed Ti/Al Ohmic contacts formed on p-type Al-implanted 4H-SiC annealed at high temperature. J. Phys. D: Appl. Phys. **44**, 255302 (2011)
3. I. Pesic, D. Navarro, M. Fujinaga, Y. Furui and M. Miura-Mattausch, Switching characteristics of a 4H-SiC insulated gate bipolar transistor with interface defects up to the nonquasi-static regime. Jpn. J. Appl. Phys. **54**, 04DP11 (2015)

4. M. Bhatnagar and B. J. Baliga, Comparison of 6H-SiC, 3C-SiC, and Si for power devices. IEEE Trans. Electron Devices **40**, 645 (1993)
5. J. Biela, M. Schweizer, S. Waffler and J. W. Kolar, SiC versus Si-Evaluation of potentials for performance improvement of inverter and DC-DC converter systems by SiC power semiconductors. IEEE Trans. Electron Devices **58**, 2872 (2011)
6. A. Itoh, T. Kimoto, and H. Matsunami, Excellent reverse blocking characteristics of high-voltage 4H-SiC Schottky rectifiers with boron-implanted edge termination. IEEE Electron Device Lett. **17**, 139 (1996)
7. S. L. Rumyantsev, M. S. Shur, M. E. Levinshtein, P. A. Ivanov, J. W. Palmour, A. K. Agarwal, B. A. Hull, and S.-H. Ryu, Channel mobility and on-resistance of vertical double implanted 4H-SiC MOSFETs at elevated temperatures. Semicond. Sci. Technol. **24**, 075011 (2009)
8. H. Yano, T. Hirao, T. Kimoto, H. Matsunami, K. Asano, and Y. Sugawara, High channel mobility in inversion layers of 4H-SiC MOSFET's by utilizing (1120) face. IEEE Electron Device Lett. **20**, 611 (1999)
9. G. Y. Chung, C. C. Tin, J. R. Williams, K. McDonald, R. K. Chanana, R. A. Weller, S. T. Pantelides, L. C. Feldman, O. W. Holland, M. K. Das, and J. W. Palmour, Improved inversion channel mobility for 4H-SiC MOSFETs following high temperature anneals in nitric oxide. IEEE Electron Device Lett. **22**, 176 (2001)
10. T. Shimizu and T. Shinohe, US Patent US2012/0199846 A1
11. M. Shimabayashi, K. Kurihara, Y. Horikawa, and K. Sasaki, Nitriding characteristics of 4H-SiC irradiated with remote nitrogen plasmas. Jpn. J. Appl. Phys. **55**, 036503 (2016)
12. M. Shimabayashi, K. Kurihara, and K. Sasaki, Suppression of carbon desorption from 4H-SiC by irradiating a remote nitrogen plasma at a low temperature. Jpn. J. Appl. Phys. **57**, 056201 (2018)
13. N. Takada, H. Ushida, and K. Sasaki, Nitridation of titanium surface by the irradiation of YAG laser pulses in N_2/O_2 gas mixture and liquid nitrogen. J. Phys. Conf. Series **59**, 40 (2007)
14. N. Takada, T. Sasaki, and K. Sasaki, Synthesis of crystalline TiN and Si particles by laser ablation in liquid nitrogen. Appl. Phys. A **93**, 833 (2008)
15. K. Sasaki and S. Harada, Excitation of cavitation bubbles in low-temperature liquid nitrogen. Jpn. J. Appl. Phys. **56**, 068002 (2017).
16. K. Fukuda, M. Kato, K. Kojima, and J. Senzaki, Effect of gate oxidation method on electrical properties of metal-oxide-semiconductor field-effect transistors fabricated on 4H-SiC C(0001) face. Appl. Phys. Lett. **84**, 2088 (2004)
17. T. Kimoto, Y. Kanzaki, M. Noborio, H. Kawano, and H. Matsunami, Interface properties of metal-oxide-semiconductor structures on 4HSiC0001 and (1120) formed by N_2O oxidation. Jpn. J. Appl. Phys. **44**, 1213 (2005)
18. R. B. Bird, W. E. Stewart, and E. N. Lightfoot, *Transport Phenomena, 2nd Ed*, John Wiley& Sons (2007)
19. L. J. Kroko and A. G. Milnes, Diffusion of nitrogen into silicon carbide single crystals doped with aluminum. Solid-State Electron. **9**, 1125 (1966)
20. P. G. Neudeck, SiC Technology. in *The VLSI HandbookBook*, Chap. 6, CRC Press, Boca Raton (2000)
21. Z. Tian, I. A. Salama, N. R. Quick, and A. Kar, Effect of different laser sources and doping methods used to dope silicon carbide. Acta Mater. **53**, 2835 (2005)
22. A. Ikeda, D. Marui, H. Ikenoue, and T. Asano, Nitrogen doping of 4H-SiC by KrF excimer laser irradiation in liquid nitrogen. Jpn. J. Appl. Phys. **54**, 04DP02 (2015)
23. R. T. Dolloff, Research study to determine the phase equilibrium relations of selected metal carbides at high temperatures. Wadd Technical Report 60-143 (1960)
24. M. Togaya and S. Sugiyama, Melting behavior of β-SiC at high pressure. Rev. High Pressure Sci. Technol. **7**, 1037 (1998)
25. T. T. P. Nguyen, R. Tanabe, and Y. Ito, Laser-induced shock process in under-liquid regime studied by time-resolved photoelasticity imaging technique. Appl. Phys. Lett. **102**, 124103 (2013)
26. T. T. P. Nguyen, R. Tanabe, and Y. Ito, Influences of focusing conditions on dynamics of laser ablation at a solid-liquid interface. Appl. Phys. Express **6**, 122701 (2013)

Fig. 1 Schematic of experimental apparatus. The fourth harmonics of a Nd:YAG laser was guided into a liquid nitrogen container with optical windows using mirrors. A lens was used for focusing the laser beam onto a 4H-SiC target which was immersed in liquid nitrogen. The lens was installed in a vacuum vessel which was necessary for the thermal isolation.

Fig. 2 SEM images of the sample (4H-SiC) surface with different magnification ratios. The laser fluence was 6.2 J/cm^2

Fig. 3 Concentration of nitrogen on the sample surface as a function of the laser fluence.

Fig. 4 Depth profiles of element concentrations (a) at the center of the ablation crater and (b) at a lateral distance of 1 mm from the crater center.

Fig. 5 Depth profiles of weight density at the center of the ablation crater and at a lateral distance of 1 mm from the crater center.

Fig. 6 Depth profiles of the number density of nitrogen at the center of the ablation crater and at a lateral distance of 1 mm from the crater center.

Fig. 7 Normal probability plot of the depth profile of the nitrogen number density observed at a lateral distance of 1 mm from the crater center.

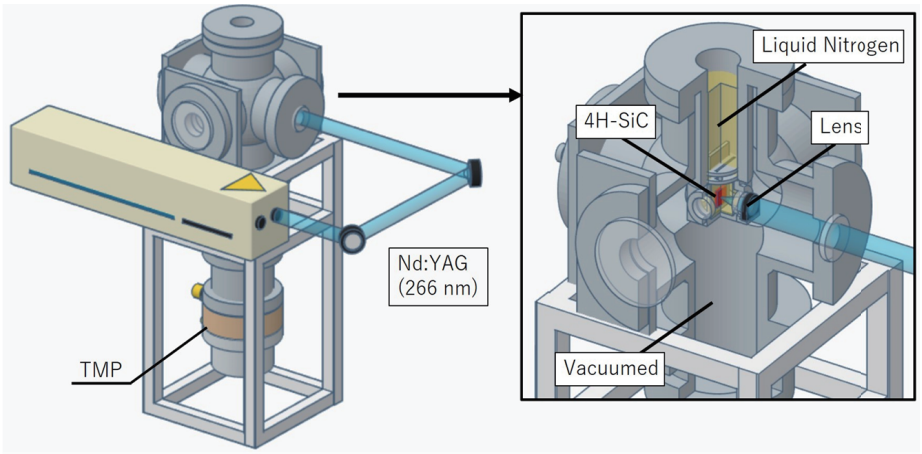

Fig. 1 Schematic of experimental apparatus. The fourth harmonics of a Nd:YAG laser was guided into a liquid nitrogen container with optical windows using mirrors. A lens was used for focusing the laser beam onto a 4H-SiC target which was immersed in liquid nitrogen. The lens was installed in a vacuum vessel which was necessary for the thermal isolation.

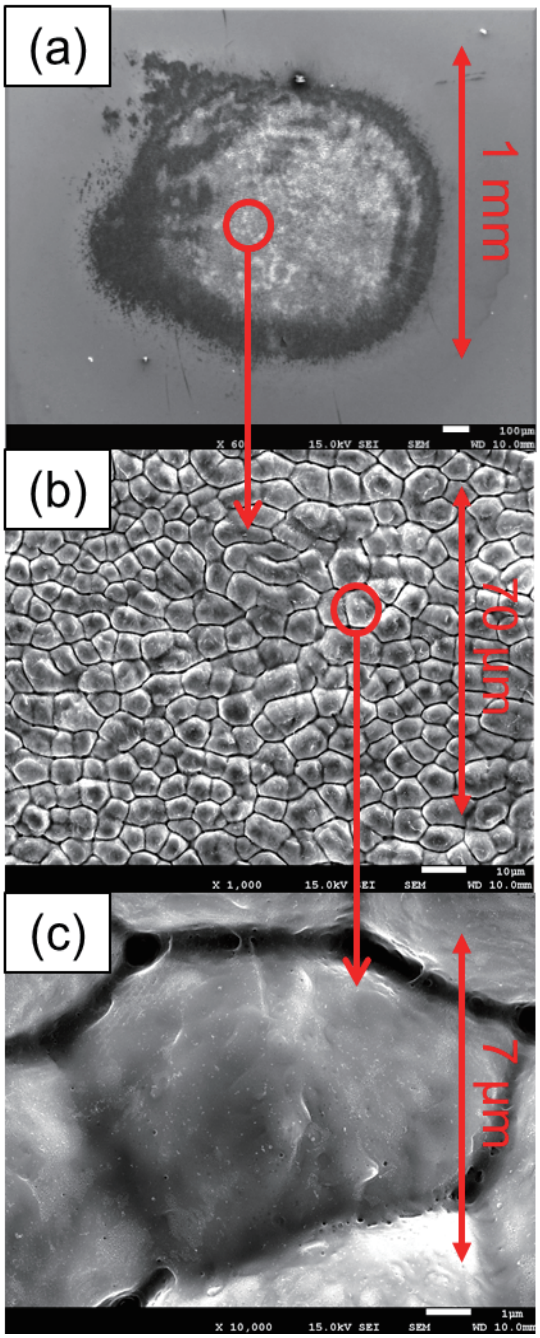

Fig. 2 SEM images of the sample (4H-SiC) surface with different magnification ratios. The laser fluence was 6.2 J/cm^2

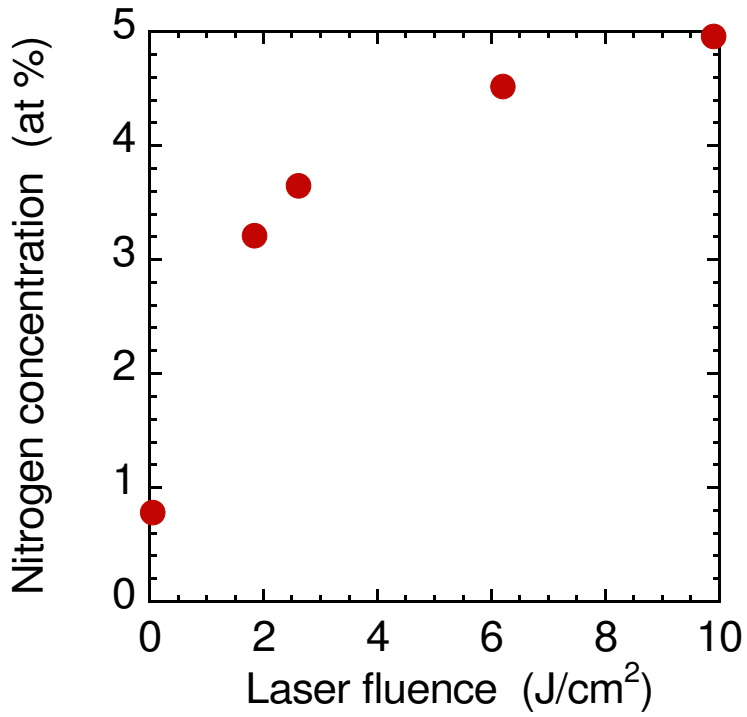

Fig. 3 Concentration of nitrogen on the sample surface as a function of the laser fluence.

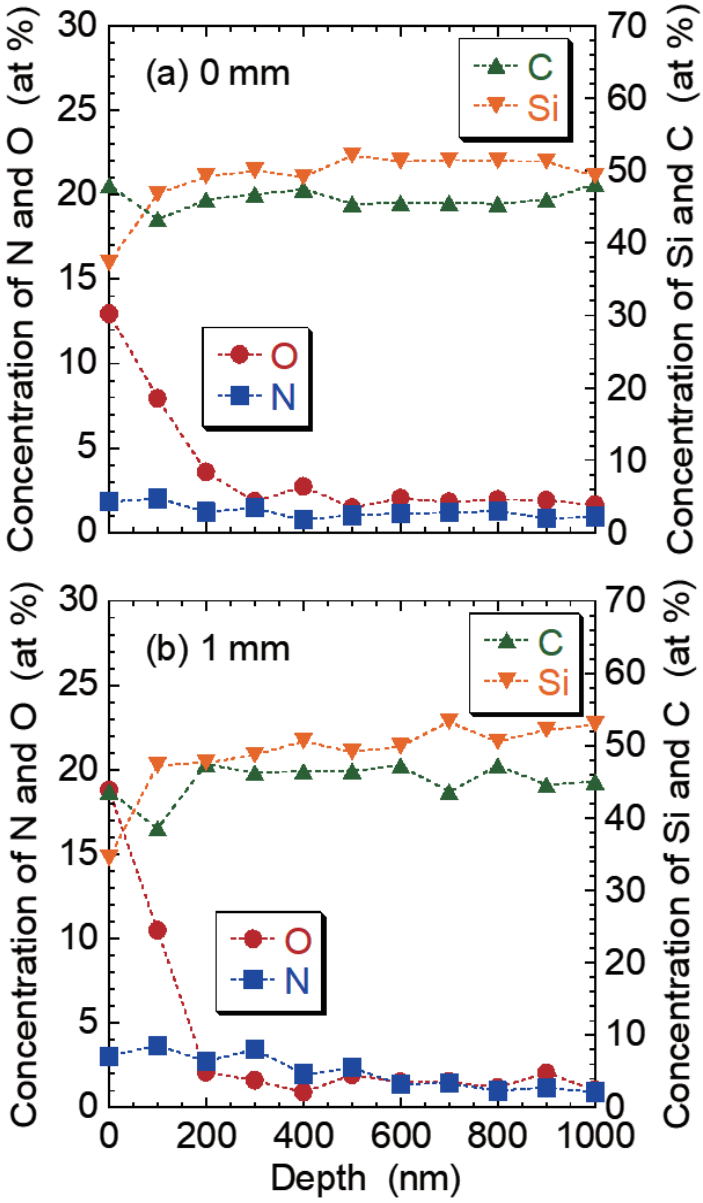

Fig. 4 Depth profiles of element concentrations (a) at the center of the ablation crater and (b) at a lateral distance of 1 mm from the crater center.

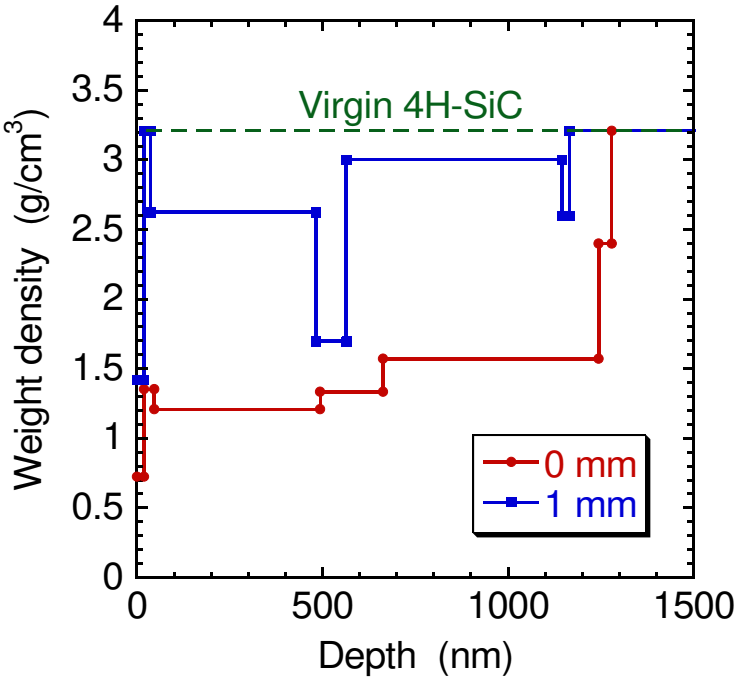

Fig. 5 Depth profiles of weight density at the center of the ablation crater and at a lateral distance of 1 mm from the crater center.

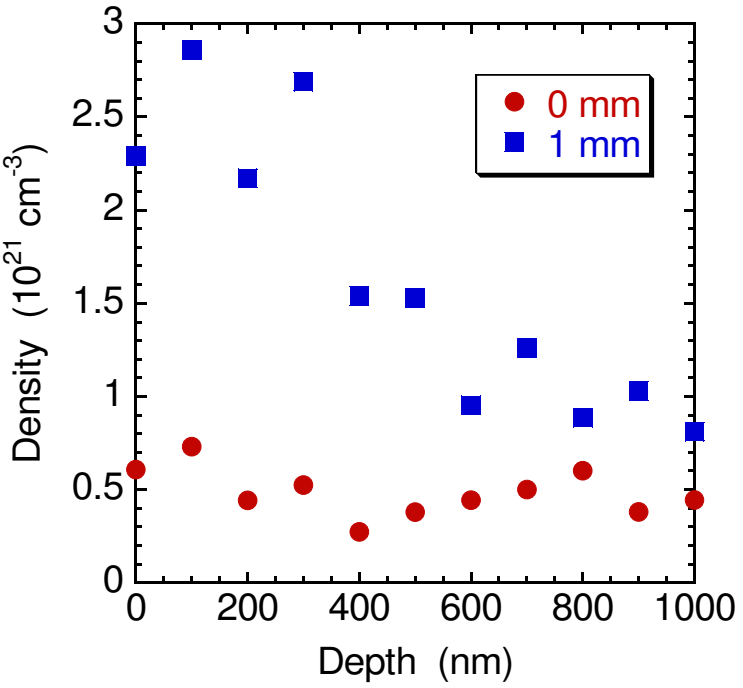

Fig. 6 Depth profiles of the number density of nitrogen at the center of the ablation crater and at a lateral distance of 1 mm from the crater center.

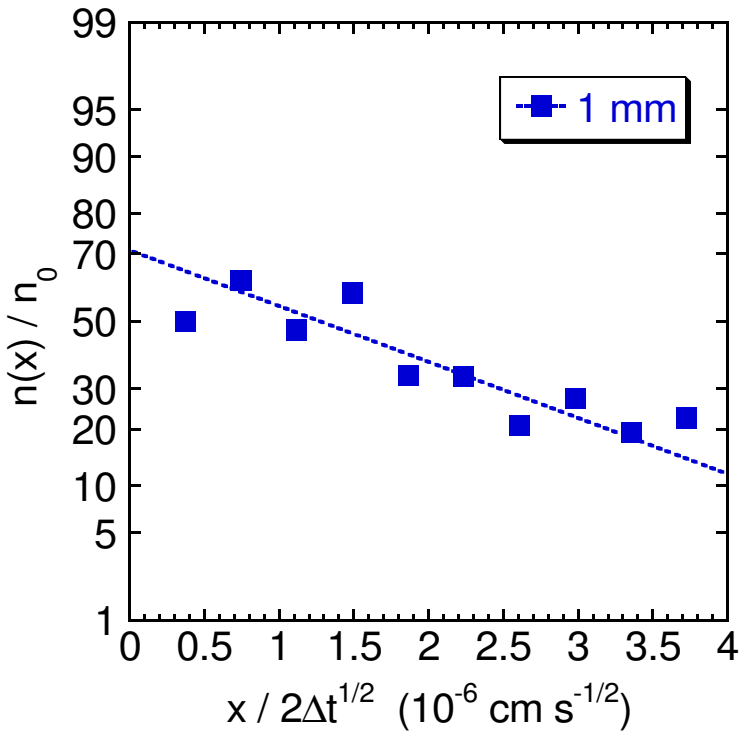

Fig. 7 Normal probability plot of the depth profile of the nitrogen number density observed at a lateral distance of 1 mm from the crater center.